MOUNTAIN-PLAINS CONSORTIUM

MPC 24-568 | W. Abdalrwaf, I. Bouzaid and P. Heyliger

SEAMLESS COMPARATIVE MODELING OF NATURAL HAZARDS USING THE MATERIAL POINT METHOD

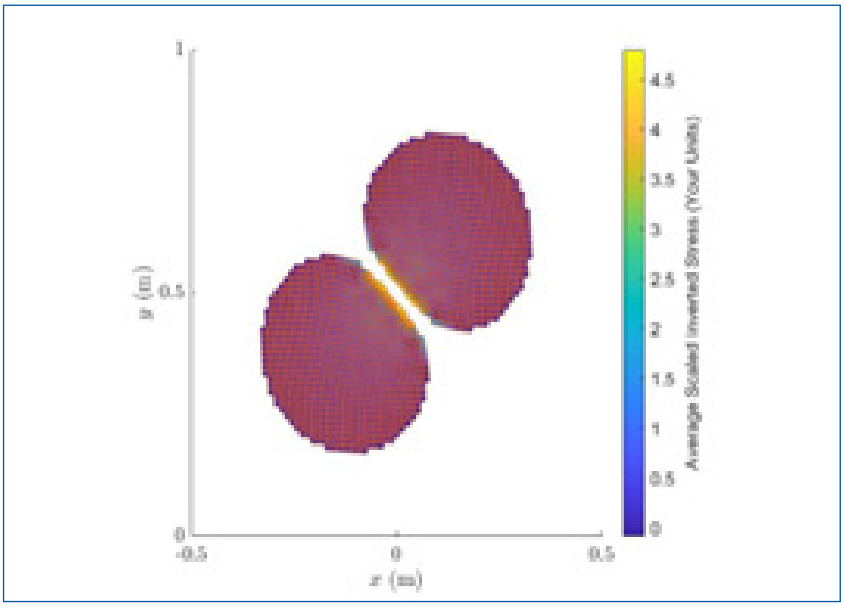

MOUNTAIN-PLAINS CONSORTIUM REGION 8

A University Transportation Center sponsored by the U.S. Department of Transportation serving the Mountain-Plains Region. Consortium members:

Colorado State University
North Dakota State University
South Dakota State University
University of Colorado Denver
University of Denver
University of Utah
Utah State University
University of Wyoming

Technical Report Documentation Page

1. Report No.	2. Government Accession No.	3. Recipient's Catalog No.
MPC-645		

4. Title and Subtitle	5. Report Date
Seamless Comparative Modeling of Natural Hazards Using the Material Point Method	October 2024
	6. Performing Organization Code

7. Author(s)	8. Performing Organization Report No.
Wael Abdalrwaf Ibrahim Bouzaid Paul Heyliger	MPC 24-568

9. Performing Organization Name and Address	10. Work Unit No. (TRAIS)
Colorado State University Department of Civil and Environmental Engineering Fort Collins, CO 80523	11. Contract or Grant No.

12. Sponsoring Agency Name and Address	13. Type of Report and Period Covered
Mountain-Plains Consortium North Dakota State University PO Box 6050, Fargo, ND 58108	Final Report
	14. Sponsoring Agency Code

15. Supplementary Notes

Supported by a grant from the US DOT, University Transportation Centers Program

16. Abstract

A theoretical framework is developed for applying the material point method (MPM) to problems of modeling natural hazard effects on several representative geometries. Following an outline of the general methodology, in which the structural system is replaced by a combination of integrated Lagrangian point masses that can move through Eulerian space, examples are shown for 1) the large deformation behavior of beam-like structures, 2) the impact between two particles, and 3) the failure of a granular slope. Key aspects of this work and approach include the ability to model large deformations, the ease of incorporating nonlinear constitutive relations, the ability to model everything from either continuous solids to granular media, and an approach to model multiple materials in the same analysis. Eventually, these computational tools can be combined with imaging methods to track the analysis of the original physical system mapped to an MPM domain using point cloud, rather than continuous, photographic imaging.

17. Key Word	18. Distribution Statement
bridges, debris flows, fluid dynamics, geological events, hazards, hydrologic phenomena, infrastructure, loads, materials, meteorological phenomena, methodology, mud, predictive models, retaining walls, risk assessment, rockfalls, simulation	Public distribution

19. Security Classif. (of this report)	20. Security Classif. (of this page)	21. No. of Pages	22. Price
Unclassified	Unclassified	35	n/a

Seamless Comparative Modeling of Natural Hazards Using the Material Point Method

Wael Abdalrwaf
Ibrahim Bouzaid
Paul Heyliger

Department of Civil and Environmental Engineering
Colorado State University
Fort Collins CO 80523

October 2024

Disclaimer

The contents of this report reflect the views of the authors, who are responsible for the facts and the accuracy of the information presented. This document is disseminated under the sponsorship of the Department of Transportation, University Transportation Centers Program, in the interest of information exchange. The U.S. Government assumes no liability for the contents or use thereof.

ABSTRACT

A theoretical framework is developed for applying the material point method (MPM) to problems of modeling natural hazard effects on several representative geometries. Following an outline of the general methodology, in which the structural system is replaced by a combination of integrated Lagrangian point masses that can move through Eulerian space, examples are shown for 1) the large deformation behavior of beam-like structures, 2) the impact between two particles, and 3) the failure of a granular slope. Key aspects of this work and approach include the ability to model large deformations, the ease of incorporating nonlinear constitutive relations, the ability to model everything from either continuous solids to granular media, and an approach to model multiple materials in the same analysis. Eventually, these computational tools can be combined with imaging methods to track the analysis of the original physical system mapped to an MPM domain using point cloud, rather than continuous, photographic imaging.

TABLE OF CONTENTS

LIST OF FIGURES

1. INTRODUCTION

Floods, landslides, and debris flows are more common every year as a result of a variety of issues, including global climate change, ecological and environmental imbalances, rising human density, urbanization, deforestation, and desertification. Additionally, both the population affected, and the resulting financial losses are growing.

A river's flow may be blocked by landslides and debris flows brought on by severe rains or earthquakes, which can naturally construct a landslide dam. One of the most significant natural hazards in mountainous areas worldwide is the formation and failure of landslide dams. Flooding from a landslide dam could inundate an area upstream that is at risk of submersion while flooding from a probable dam failure could occur downstream. To assess the flooding area and potential hazards downstream in the case of catastrophic failure of a landslide dam, the subsequent outflow hydrograph must be forecasted. Only then can proper safety precautions be taken. Subsequently, various research projects have attempted to define the processes, hazards, and mitigating measures associated with landslide damming and failure [3].

A landslide dam might last anywhere from a few seconds to a few thousand years. It is very challenging to forecast whether or when a dam may fall once it has formed. Therefore, for efficient hazard management, it is crucial to understand how the characteristics of a landslide dam affect the peak output of the ensuing dam-break floods. Understanding the temporal and spatial scales on which such occurrences occur is crucial for managing threats. Numerous earlier investigations on landslide dams have mostly been descriptive and resulted in a wealth of case studies and inventory that are well-documented [14, 15] Recent research has concentrated on quantitative techniques for identifying the post-formation development, particularly the controls on dam lifetime [18, 34, 35, 41, 46].

A landslide dam may suddenly collapse due to overtopping gradually over time or because of erosion. Even though there has been much engineering research on human-made dams, the failure mechanisms of landslide dams are rather well understood, but there has been very little direct observation of these failure processes. When compared with erosion brought on by overtopping, the peak discharge caused by a rapid dam collapse is very high. Nevertheless, a deep understanding of the dam failure mechanism and measured data are still lacking. Despite significant variations in dam shape and material qualities, landslide dam failure is still routinely treated as a homogenous earthen dam failure because the mechanism of breach generation is thought to be quite similar. The majority of the currently used models are suitable for landslide dam overtopping failure.

A landslide dam's catastrophic failure could happen soon after it is formed. For the management of dam-break flood dangers and to choose appropriate mitigation measures, including evacuation, quick forecasting of the possible peak discharge is required. Using empirical regression relationships based on the amount of the dammed lake and the estimated height of the dam, preliminary peak discharge may be calculated. After gathering precise data on dam geometry, soil qualities, topography, and inflow discharge, physical-based computer models can be applied.

Although dam failure is a significant aspect of this work, it is also important to be able to understand and represent the basic behavior of either continuous solids and particles/structures under impact with each other. Finite element models are useful for these sorts of structures, but one of the benefits of the MPM is to be able to model these basic structural elements.

The purpose of this research is to develop a graphical relationship to predict landslide failure modes caused by landslide dam failure due to overtopping and sliding. This will be accomplished by numerically simulating a non-cohesive, homogeneous landslide.

2. THEORY

In this section, the basic elements of the material point method (MPM) are described. Historically, there are several other mesh-free/mesh-less frameworks available. Since starting with the early smoothed particle hydrodynamic (SPH), which Gingold and Monaghan [19] and Lucy [39] presented, there have been issues with modeling astrophysical processes. Liszka and Orkisz [37] later created a finite difference technique, while Nayroles, Touzot, and Villon [43] created the diffuse element method (DEM), which led to the Sulsky et al. [51] material point approach, which is used in this study.

One of the improved mesh-less methods is the MPM, which is regarded as an extension of Harlow's [24] particle-in-cell (PIC) method for fluid mechanics modeling. However, PIC has an energy dissipation problem, which affects the method's accuracy. Brackbill and Ruppel [8] established the fluid implicit particle method (FLIP), which was developed initially for fluid simulation. Sulsky et al. [51, 52] later provided a modification of this method for use in solid mechanics formulation. Sulsky and Schreyer [50] then named this modification the material point method.

As shown in Figure 2.1, the MPM concept is based on two field descriptions: the Lagrangian description and the Eulerian grid. In the MPM, a continuum body is discretized into multiple numbers of particles named points. These are known as Lagrangian material particles. The Lagrangian description of particles implies that they are ingrained in and deformed by the material. Position, mass, density, volume, deformation gradient, and Cauchy stress tensor are all attributes of each particle. Throughout the process, the particle's mass remains constant, but the material's deformation causes its volume to change. Throughout the deformation procedure, these particles are evaluated. The continuum body's background mesh/grid allows it to deform in the same grid that describes Sulsky's updated Lagrangian scheme, where the equation of momentum is also solved. However, the continuum body only fills the background grids/mesh in the reference configuration in the total Lagrangian material point method (TLMPM) developed by de Vaucorbeli et al. [9].

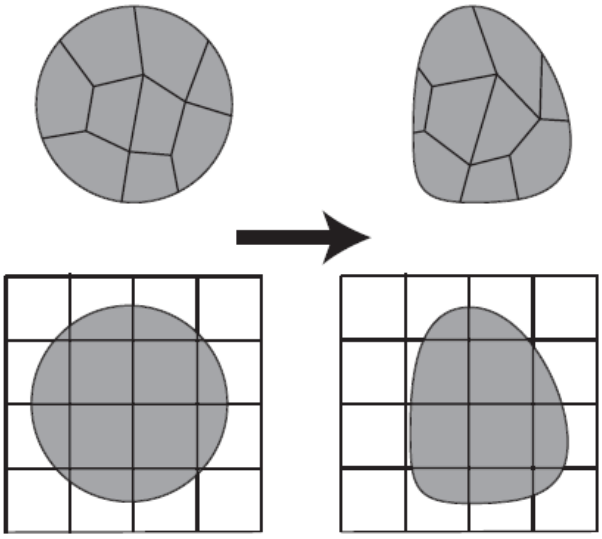

Figure 2.1 The Lagrangian description (top) and Eulerian grid (bottom) [17]

The MPM algorithm was first developed to examine some simple solid mechanics problems [51]. As a result, various MPM algorithms have been developed to explicitly solve such problems, providing more effective processes than implicit ones. The updated Lagrangian MPM approach considers the explicit solutions to be the simplest form. However, with the same straightforward modification, the TLMPM can be created from the updated Lagrangian MPM. The first step in the MPM general algorithm is to transfer (map) the particle information to the grid, as shown in Figure 2.2. The nodes are then used to solve the momentum balance equation.

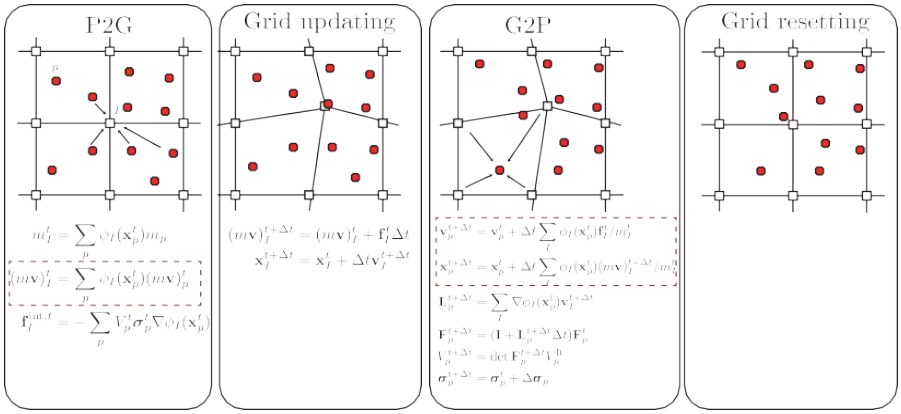

Figure 2.2 Material point method general computational steps [17]

All the particles' information and variables, including their positions, volumes, densities, stresses, and other qualities, are updated from the node to the particles. The grid eventually reconstructs to its original state. This final reconstruction prevents distortion from occurring, allowing the MPM to be a suitable approach for large deformation problems such as slope failure.

Few algorithms have been developed since the MPM's introduction; the standard material point algorithm developed by Sulsky et al. [51] is the updated stress last (USL). This method does, however, produce a numerical problem related to the mass of the small particles. To avoid the small mass issue, Sulsky et al. [52] extended the formulation to the modified updated stress last (MUSL), where the updated particles' velocity is mapped back to the nodes. De Vaucorbeli et al. [16] also developed the TLMPM formulation to track nonlinear behavior under large load impact.

The MPM has a few advantages that make it a good choice for modeling such problems. One of the advantages is the loss of mesh, as the particles carry the analyzed information. Furthermore, because Eulerian mesh/grids cover the entire deformable domain, they allow for direct and efficient treatment of multi-body frictional contacts. While MPM has a simpler computer implementation than other meshless methods, it also produces high-quality images and simulations. Due to the similarity of the finite element method (FEM) and MPM, the influence of wide FEM studies supports the MPM to be considered.

3. APPLICATIONS

This section contains several representative applications considered using the MPM. This particle-based approach is known for handling large deformation problems in solid mechanics. However, MPM has not been widely used for studying the static response of solid structures because it excels at modeling complex interactions, which are common in geotechnical and fluid engineering fields. Recently, de Vaucorbeli et al. [17] noted a lack of MPM studies on structural elements like beams and shells, highlighting a significant gap in the research.

This study aims to fill this gap by examining the static response of cantilever beams using MPM. The focus is on how particles behave under different conditions, including changes in geometry and material properties such as the modulus of elasticity and Poisson's ratio. The results from MPM will be compared with analytical solutions from linear elasticity theory, particularly those developed by Timoshenko and Goodier [67].

The research will explore how different loading conditions and beam shapes affect the accuracy of MPM compared with traditional methods. It will also look at how the number of material points used in the model impacts the results. By tracking the behavior of the beam at various points, the study aims to provide a clear understanding of how well MPM can predict static deformations.

Ultimately, this research seeks to demonstrate that MPM is a valuable tool for analyzing large deformations in structural elements. By validating MPM against well-known analytical solutions, the study will show its potential for broader applications in structural mechanics, paving the way for future research into more complex deformation problems.

In the realm of material mechanics, the behavior of two-elastic materials presents a critical research domain. While the MPM has proven its prowess in addressing large deformation challenges, there exists a notable gap in the exploration of how MPM can be applied to comprehensively understand the behavior of materials with dual elasticity. This research seeks to fill this void by undertaking a systematic investigation into the dynamic response, deformation patterns, and failure mechanisms of structures composed of two-elastic materials.

The primary objectives include formulating a sophisticated two-dimensional MPM model within the MATLAB environment, tailored explicitly to capture the nuanced intricacies of bars constructed from two-elastic materials. The precision in defining parameters, such as the Eulerian grid size and the optimal particle distribution across the undeformed domain, is paramount to ensure accurate simulations. The research further delves into understanding the influence of diverse material constants and varying particle numbers on the behavior of two-elastic materials, unraveling the model's sensitivity to a spectrum of parameters. The eventual establishment of a comprehensive material point model dedicated to the impact of two-elastic materials is poised to contribute valuable insights to the broader context of material mechanics.

The simulation of slope failure in dams emerges as a crucial facet in the domain of geotechnical engineering. While meshless methods offer conceptual advantages in capturing large deformation problems, their susceptibility to instability and numerical fracture poses challenges in accurately modeling scenarios like slope failures. This research embarks on the development

of a specialized two-dimensional material point model in MATLAB, meticulously crafted for simulating the intricate dynamics of slope failure in dams.

The definition of the Eulerian grid size, coupled with the determination of an optimal number of particles, becomes a focal point to ensure the faithfulness of the model's representation of the physical system. An exploration into the influence exerted by varying material point numbers and particle distributions on the slope failure domain aims to provide nuanced insights into the robustness of the model. The research further extends to systematically track the impact of deformation stemming from different geometries and boundary conditions, offering a comprehensive understanding of slope behavior under diverse scenarios.

The emulation of dam collapses stands as a critical area of study within structural engineering. The TLMPM, known for its efficiency in handling very large deformations, becomes a central component in addressing the intricacies associated with the unique characteristics of dam structures. This research endeavors to formulate a rigorous two-dimensional TLMPM, explicitly designed to capture the complex dynamics and failure modes intrinsic to dam collapse.

The precision in defining stress and strains in the reference configuration, coupled with the utilization of nonlinear constitutive equations, forms the backbone of TLMPM's effectiveness in tracking large deformations. Its resistance to cell-crossing errors and numerical fractures positions TLMPM as an efficient formulation for studying structural behavior. The research methodology aims to study the structure's behavior using TLMPM under various load and geometry assumptions. This comprehensive exploration aspires to contribute valuable insights to the scholarly understanding of dam collapses and advance the application of computational mechanics in addressing critical challenges in structural engineering.

In the MUSL algorithm, Sulsky et al. [59] proposed a solution to address the issue associated with small masses.

Meshless methods present viable concepts for the simulation of large deformation problems in solid mechanics, offering advantages over mesh-based counterparts. However, it is noteworthy that meshless methods are prone to instability issues and numerical fracture, rendering them less accurate for the analysis of engineering scenarios involving phenomena like machining, wear, and impacts, where damage and fracture mechanisms are prevalent [9].

The total Lagrangian particle-based methods demonstrate resistance to numerical fracture, attributed to the stability maintained by the background grids in the reference configuration throughout the analysis. Leveraging this stability, the TLMPM was introduced by Steffen et al. [55], initially for the convergence study of the standard MPM. Subsequently, Zhu et al. [65] employed TLMPM for graphic simulation purposes.

In the scholarly continuum of structural mechanics research, seminal contributions from Timoshenko and Goodier; Lekhintskii, Pagano, Gere, and Timoshenko; and others have laid the foundational groundwork for our comprehension of linear elastic material theory. Subsequent investigations, building upon this formidable edifice, have probed more intricately into the discipline, directing their focus toward two pivotal dimensions: large deformation and elastic deformation.

The important work by Chucheepsahul, Bunacharoen, and Huang [68] develops as a noteworthy exploration into the intricacies of large deformation. This meticulous study, which centered on beams experiencing pronounced deformations, not only underscores the imperative of integrating large deformation paradigms into analytical frameworks but also yields exact solutions. Of particular note is the confluence of these outcomes with finite element analysis and linear theory, explaining the fundamental role of large deformation considerations for precision in elasticity solutions.

Ma et al.'s research [69] significantly expands the understanding of large deformation by understanding the Timoshenko beam theory of dynamic response analysis. The nuanced definition of limitations within classical models, when confronted with the challenge of capturing natural frequencies under large deformations, represents a pivotal contribution. Furthermore, their judicious consideration of Poisson ratio impact and size effects highlights the intricate interplay between material properties and large deformation behavior.

Andersen and Andersen's scholarly contribution [70], marked by a comparative analysis of the MPM against elasticity solutions, is exemplary in this academic pursuit. Their comprehensive investigation crossed a spectrum of linear elastic problems, meticulously delineating MPM's efficiency in modeling elastic deformations within the continuum mechanics framework. The discernible reduction in error with escalating order of interpolation underscores the method's acumen in handling the complexities inherent in elastic deformation scenarios. A representative example is shown in Figure 3.1, where a 6-meter cantilever beam is studied under large deformation.

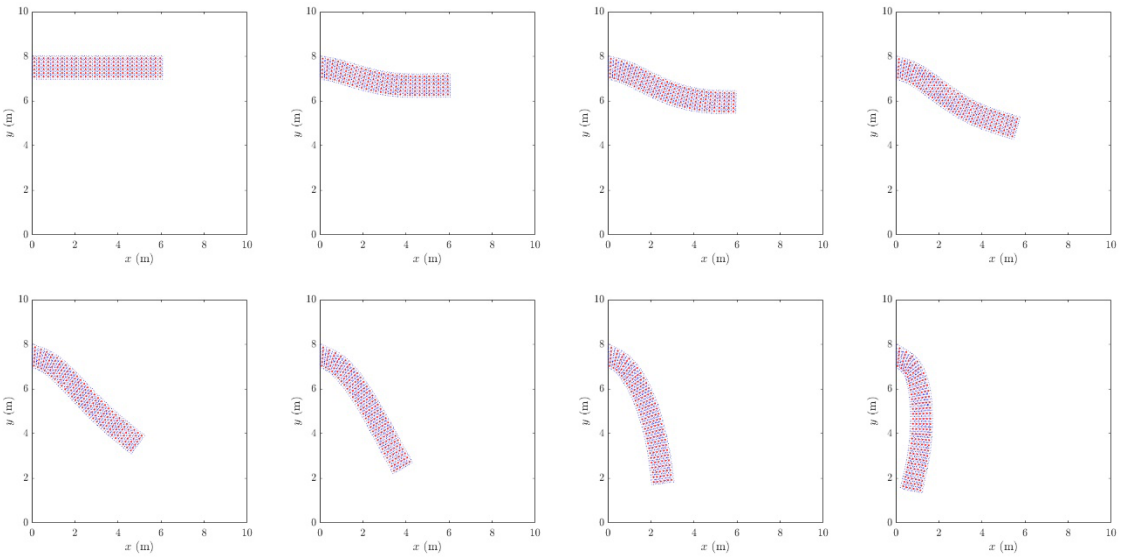

Figure 3.1 Cantilever beam simulations under large deformation using TLMPM

Hydrocodes are typically used to examine certain physical phenomena brought on by impact and penetration, such as non-linear wave propagation, friction and abrasion, significant deformation, dynamic damage, and fracture [30]. Anderson [2] and Benson [5] have examined the wide variety of hydrocodes that are currently available. Traditionally, Lagrangian and Eulerian methods have been used to construct hydrocodes for impact and penetration simulations. The analysis of material interfaces and free interfaces is problematic for Eulerian approaches. In order to model the impact and penetration issues, a sibling boundary layer interface algorithm (BLINT) for sliding interfaces was included in the Eulerian CTH hydrocode [45, 48].

In the field of solid mechanics, Lagrangian [10, 11] and arbitrary Lagrangian-Eulerian methods [38] have been widely used to simulate penetration. The penetration has been simulated using the Lagrangian finite element method (FEM) based on rate-dependent plasticity, explicit contact/friction algorithm, and adaptive meshing [11]. Despite having the ability to trace material interfaces, Lagrangian codes can cause mesh distortion and entanglement while simulating penetration. In order to model penetration, Lagrangian codes frequently include a non-physical element erosion method. Recent meshless approaches, such as smoothed particle hydrodynamics (SPH) [32], meshless local Petrov-Galerkin method [23], and MPM [51, 52], have been used to handle problems involving impact and penetration.

The MPM, developed by Sulsky et al. [51, 52], is a solid mechanics application of the particle-in-cell approach [9, 25]. It discretizes a material domain using a set of material points since it is a completely Lagrangian particle approach. The grid distortion and entanglement are entirely avoided by solving the momentum equations on a predetermined uniform backdrop grid. The upsetting process [49], Taylor bar impact [50], dynamics crack [22, 53], explosive process [21, 28], hypervelocity impact [40, 61], and dynamic analysis of saturated porous media [60] are only a few of the challenging engineering issues that MPM has been used to solve. Even though MPM has been used to overcome hypervelocity issues, simulating penetration issues with MPM is still a challenging process.

The conventional MPM algorithm prevents material particle interpenetration by applying single-valued mapping functions between background grid nodes and particles. The common MPM includes a no-slip contact condition by default. A typical MPM simulation was run by Sulsky et al. [52] for a steel sphere striking an aluminum target at 1,160 m/s. They discovered that the usual MPM's calculation of penetration depth is significantly off from the outcome of the experiment. Therefore, an effective contact algorithm for releasing no-slip contact should be created. In some cases, involving impact and penetration, the inherent no-slip contact condition in the typical MPM may result in larger penetration resistance.

York et al. [59] suggested a straightforward contact algorithm to enable the removal of the no-slip contact requirement in the conventional MPM. In York's method, the impenetrability criterion is imposed using the normal MPM method if the bodies are in contact with one another. The bodies move in their velocity fields to allow separation if they are traveling apart from one another. Hu and Chen [27] introduced a contact/sliding/separation algorithm in the multi-mesh environment to prevent interpenetration and permit separation in the gear contact process. The normal velocity of each material particle at the contact surface is determined by their contact algorithm using the shared background grid; however, the tangential velocity is determined using

the corresponding individual grid. Although the contact algorithms outlined above are effective at separating contact bodies, friction is not considered.

In multi-velocity fields, a contact/friction/separation strategy was presented by Bardenhagen et al. [4, 20]. When contact occurs, MPM incorporates the impenetrability requirement and the Coulomb friction between bodies. The relative nodal velocity at the contact surface is used to calculate the contact force between two entities. The method has been proven using the granular shearing simulation and the sphere rolling on an inclined plane [20]. A recent three-dimensional multi-mesh contact algorithm for MPM was proposed by Pan et al. [58]. In this contact algorithm, the normal nodal acceleration continuity requirement at the contact surface is used to calculate the contact force between the bodies.

The backdrop grid is used in MPM to apply the contact conditions, and the nodal variables can fully characterize the contact issues. A general formulation of the contact-impact problem is offered in this study. In the technique, the impenetrability condition is only placed on the deformed grid after each time step, as opposed to being imposed on both the deformed grid and the redefined regular grid at the start of the subsequent time step. The contact approach is used to simulate the penetration of two elastic balls using a particle failure model.

This section outlines the contact resolution algorithm proposed by Bardenhagen et al. [4] designed specifically for deformable bodies. To streamline the discussion, we initially address contact scenarios involving both deformable bodies and rigid bodies, with subsequent consideration for self-contact as an added layer of complexity. Conceptually, the contact algorithm functions as a predictor-corrector scheme. Initially, nodal velocities are predicted independently for each body, treating them as if no contact has occurred. Subsequently, these predicted velocities undergo correction using a contact model. Note that the contact algorithm is selectively applicable to contact nodes, defined as those nodes receiving contributions from particles belonging to more than one body, as illustrated in Figure 3.2. For simplicity, our focus remains on contacts between distinct bodies, while self-contact requires specialized treatment, as detailed in Homel and Herbold. [6464]

For each body indexed as $k = 1, 2, \dots n$, where n denotes the total number of bodies, the standard MPM problem is systematically addressed.

$$m_I^{t,(k)} = \sum_{p=1}^{n_p^k} \varphi_{Ip} m_p \,,\; v_I^{t,(k)} = \frac{1}{m_I^{t,(k)}} \sum_{p=1}^{n_p^k} \varphi_{Ip} m_p v_p \,,\; a_I^{t,(k)} = \frac{f_I^{(k)}}{m_I^{t,(k)}} \qquad 5.2.1$$

$$\tilde{v}_I^{t+\Delta_t,(k)} = v_I^{t,(k)} + \Delta_t a_I^{t,(k)} \qquad 5.2.2$$

Where, n_p^k signifies the count of particles constituting body k. It is imperative to highlight that the velocity field represented by a tilde is provisional and necessitates correction specifically for contact nodes. The corrected velocity, denoted as $v_I^{t+\Delta_t,(k)}$ (without a tilde), subsequently becomes the foundation for updating particles' stress, position, and velocity, adhering to rigorous engineering principles.

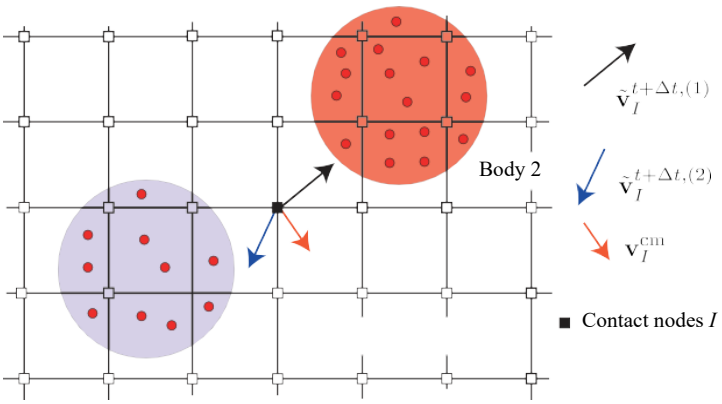

Figure 3.2 Two bodies make contact; nodes in contact or overlapping (represented by black solid squares) are defined as those that receive contributions from particles of both bodies.

Following the computation of $\tilde{v}_I^{t+\Delta_t,(k)}$, the subsequent step involves detecting, particularly at contact nodes, whether two bodies are approaching or departing from each other. For simplicity, the subsequent presentation focuses on the interaction between two bodies, although the algorithm itself is versatile and can be extended to accommodate multiple bodies. Bardenhagen et al. [4] introduced a linear algorithm, denoted as

$$\left(\tilde{v}_I^{t+\Delta_t,(k)} - v_I^{cm}\right) \cdot n_I^{(k)} = \begin{cases} \geq 0 & contact \\ < 0 & release \end{cases} \qquad 5.2.3$$

applicable to the number of bodies involved. This algorithm utilizes v_I^{cm}, known as the center of mass velocity field, derived as

$$v_I^{cm} = \frac{(m_I \tilde{v}_I)^{t+\Delta_t,(1)} + (m_I \tilde{v}_I)^{t+\Delta_t,(2)}}{m_I^{t,(1)} + m_I^{t,(2)}} \qquad 5.2.4$$

from the combined contributions of particles from the two bodies. This resultant velocity is referred to as the system velocity field. The algorithm's efficacy lies in its departure from considering pairwise interactions of bodies, opting instead for a common frame defined by global quantities. This allows for simultaneous contact resolution across all bodies.

If equation *(5.2.3)* determines that the two bodies are approaching, a correction to the velocities $\tilde{v}_I^{t+\Delta_t,(k)}$ is necessary to obtain the final velocity $v_I^{t+\Delta_t,(k)}$. Otherwise, the velocities remain unaltered. The method for correcting grid velocities is contingent upon the specific contact model, with detailed discussions provided in earlier discussions for nonslip contact. Subsequently, particle velocities, positions, and stresses undergo updates following the equations presented below:

$$a_I^{t+\Delta_t,(k)} = \frac{v_I^{t+\Delta_t,(k)} - v_I^{t,(k)}}{\Delta_t}$$

$$x_p^{t+\Delta_t,(k)} = x_p^{t,(k)} + \Delta_t \sum_{p=1}^{n_p^k} \varphi_I\left(x_p^t\right) v_I^{t+\Delta_t,(k)}$$

$$v_p^{t+\Delta_t,(k)} = v_p^{t,(k)} + \Delta_t \sum_{p=1}^{n_p^k} \varphi_I\left(x_p^t\right) a_I^{t,(k)} \qquad 5.2.5$$

The first equation in the set calculates corrected accelerations, specifically required for contact nodes. Notably, stress updates are omitted as they adhere to standard procedures. The discussion presented aligns with the update stress last (USL) formulation.

The algorithm employed for contact-release at a given contact node I is straightforward. When contact is established, the nodal velocity undergoes correction to align the normal component of the body velocity with the normal component of the center-of-mass velocity. In the absence of friction between the bodies, this adjustment represented mathematically as

$$v_I^{t+\Delta_t,(k)} = \begin{cases} \tilde{v}_I^{t+\Delta_t,(k)} - \left[\left(\tilde{v}_I^{t+\Delta_t,(k)} - v_I^{cm}\right) \cdot n_I^{(k)}\right] n_I^{(k)}, & contact \\ \tilde{v}_I^{t+\Delta_t,(k)} & , \ release \end{cases} \qquad 5.2.6$$

in equation (*5.2.6)* suffices for effective contact treatment. Notably, the tangential component of the body velocity remains unconstrained.

The assertion that the normal component of the body velocity equates to the normal component of the center-of-mass velocity can be formally demonstrated as:

$$\begin{aligned} v_I^{t+\Delta_t,(k)} \cdot n_I^{(k)} &= \tilde{v}_I^{t+\Delta_t,(k)} \cdot n_I^{(k)} - \left\{\left[\left(\tilde{v}_I^{t+\Delta_t,(k)} - v_I^{cm}\right) \cdot n_I^{(k)}\right] n_I^{(k)}\right\} \cdot n_I^{(k)} \\ &= \tilde{v}_I^{t+\Delta_t,(k)} \cdot n_I^{(k)} - \left(\tilde{v}_I^{t+\Delta_t,(k)} - v_I^{cm}\right) \cdot n_I^{(k)} \qquad 5.2.7 \\ &= \tilde{v}_I^{t+\Delta_t,(k)} \cdot n_I^{(k)} - \tilde{v}_I^{t+\Delta_t,(k)} \cdot n_I^{(k)} + v_I^{cm} \cdot n_I^{(k)} = v_I^{cm} \cdot n_I^{(k)} \end{aligned}$$

Similarly, the confirmation that the tangential component of the corrected velocity is identical to the tangential component before correction can be proven as:

$$\begin{aligned} & v_I^{t+\Delta_t,(k)} - \left[v_I^{t+\Delta_t,(k)} \cdot n_I^{(k)}\right] n_I^{(k)} \\ &= \tilde{v}_I^{t+\Delta_t,(k)} - \left[\left(\tilde{v}_I^{t+\Delta_t,(k)} - v_I^{cm}\right) \cdot n_I^{(k)}\right] \cdot n_I^{(k)} - \left(v_I^{cm} \cdot n_I^{(k)}\right) n_I^{(k)} \qquad 5.2.8 \\ &= \tilde{v}_I^{t+\Delta_t,(k)} - \left(\tilde{v}_I^{t+\Delta_t,(k)} \cdot n_I^{(k)}\right) n_I^{(k)} \end{aligned}$$

The determination of normal vectors $n_I^{(k)}$ at grid nodes for each body constitutes a pivotal step in completing the contact algorithm, as it significantly influences the accuracy of the results. The conventional approach involves isolating each body in relation to system velocities to derive the normal vectors. This entails computing the normal from the mass gradient of the material in consideration. For each entity, the particle mass undergoes interpolation to the element centers, denoted as x_c , and is then divided by the element volume V_e to yield a density ρ_c. The gradient of ρ_c, evaluated at the grid nodes, provides the normal direction at the surface of each body (Bardenhagen et al., [4]; Sulsky & Brackbill, [63, 64]).

The cell-centered density, defined as

$$\rho_c = \frac{1}{V_e}\sum_{p=1}^{n_p} m_p S^2\left(x_p - x_c\right) \qquad 5.2.9$$

incorporates bi-quadratic B-spline functions denoted as S^2. In two dimensions, these functions are expressed as $S^2 = S^x(x)S^y(y)$, with the one-dimensional quadratic B-spline function given by

$$S^x(x) = \begin{cases} \frac{1}{2h_x^2}x^2 + \frac{3}{2h_x}x + \frac{9}{8}, & -\frac{3}{2h_x} \le x \le \frac{1}{2h_x} \\ -\frac{1}{h_x^2}x^2 + \frac{3}{4}, & -\frac{1}{2h_x} \le x \le \frac{1}{2h_x} \\ \frac{1}{2h_x^2}x^2 + \frac{3}{2h_x}x + \frac{9}{8}, & \frac{1}{2h_x} \le x \le \frac{3}{2h_x} \\ 0, & Otherwise \end{cases} \qquad 5.2.10$$

where h_x signifies the cell spacing in the x direction. B-splines on a one-dimensional mesh (Figure 3.3) typically generate particles that contribute mass and momentum to multiple approximating functions. In 2D, each particle contributes to nine cells (the center block of a 3 x 3 mesh and its neighbors), and in 3D this extends to 27 cells.

The grid normal vector is subsequently expressed as

$$n_I = \sum_c \nabla\varphi_I(x_c)\rho_c \,,\; n_I \frac{n_I}{\|n_I\|} \qquad 5.2.11$$

where $\nabla\varphi_I$ represents the gradient of the MPM weighting functions. Note that the summation is performed on cells that include the node under consideration in their connectivity, as depicted in Figure 3.4. This method of computing normals is similar to SPH (Randles & Libersky, [62]).

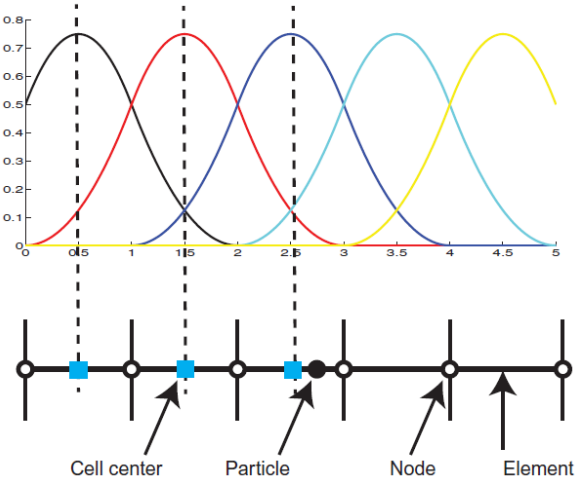

Figure 3.3 The quadratic B-spline functions utilized to define cell center density

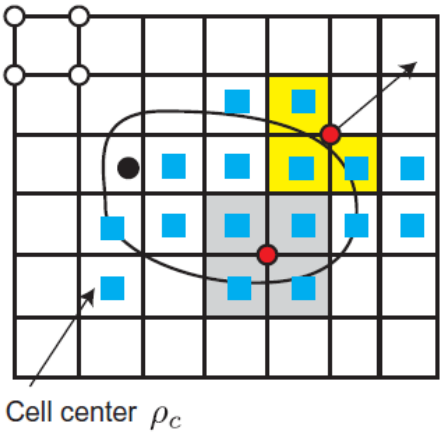

Figure 3.4 The calculation of grid normal utilizing Equation (5.1.11)

The foundational explicit TLMPM algorithm seamlessly incorporates the previously introduced contact algorithm into the conventional MPM. MPM methods for smooth contact scenarios requires a straightforward adjustment to contact force generation to accommodate Coulomb friction. While the illustration employs the update stress first (USF) approach, adapting it for the USL method is a manageable task. An integral modification to the standard MPM code involves enriching each grid node with information related to body velocity, mass, and the system's overall mass and velocity.

Figure 3.5 illustrates a representative explicit TLMPM computational cycle beginning with the mapping of particle information onto the grid (P2G). Subsequently, discrete equations of momentum are addressed on the grid nodes through the process of grid updating. Following this, particle attributes, including position, velocity, volume, density, deformation gradient, stresses, and other pertinent internal variables, undergo updates (G2P). Unlike the updated Lagrangian material point method (ULMPM) algorithm, TLMPM performs all mapping and interpolations in the undeformed reference configuration, considered as the initial state. A comprehensive flowchart of the explicit TLMPM, utilizing the modified update stress last (MUSL) formulation

proposed by Sulsky et al. [51], is encapsulated in Algorithm 1. The TLMPM's flowchart is similar to that of the ULMPM, with the notable distinction that the first Piola–Kirchhoff stress tensor is employed in the internal force vector, and spatial derivatives are taken with respect to the reference configuration, as opposed to the current (deformed) one. It is noteworthy that, for augmented robustness, the proposed modifications adhere to certain principles.

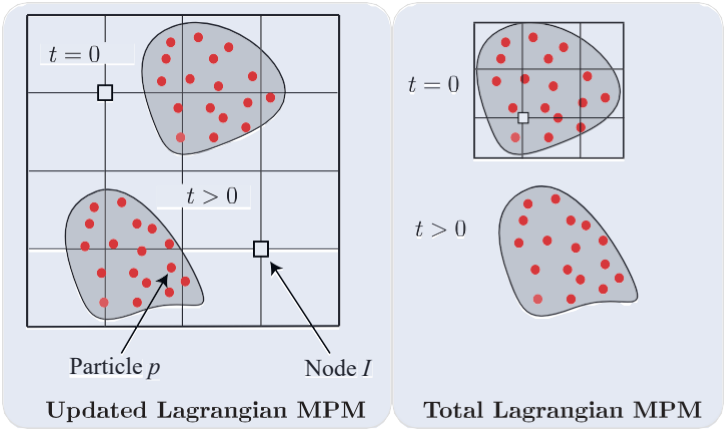

Figure 3.5 Difference between ULMPM and TLMPM

Example: Particle Contact

Preliminary results of this investigation into the collision between two elastic balls utilizing the implicit dynamic method offer a comprehensive understanding of the complexities involved in such dynamic simulations, shedding light on various critical aspects of the process. The initial examination focuses on the collision of two elastic bodies, a fundamental problem first introduced by Sulsky et al. [51]. This problem serves as a litmus test for the implementation of a 2D MPM code, offering a straightforward yet insightful scenario to validate the computational framework.

It is essential to choose the right element type for dynamic analyses in order to guarantee their accuracy and stability. Low-order components, specifically 4-node quadrilateral elements, are used in this study because high-order elements run the risk of producing negative terms in the mass matrix. The robustness and dependability of the numerical simulations are ensured by this thorough selection. Furthermore, it is found that for dynamic analysis, four material points per element are adequate to preserve accuracy. This conclusion is important because it removes the need to incorporate extra "soft stiffness," simplifying the computational model while maintaining the accuracy of the findings.

As shown in Figure 3.6, core simulation contains two elastic balls, each with a radius of 0.2 aspect ratio thickness/width, functioning under plane strain conditions. These balls are first placed at opposing corners of a square background mesh made up of 100 x 100 equal-sized square components (elements resulting in a total of 1,624 particles).

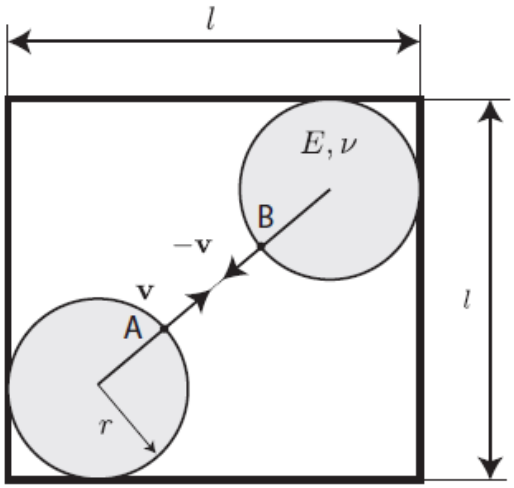

Figure 3.6 Impact of two elastic bodies: problem statement. The computational domain is a unit square, and the radius of the disks is 0.2 mm. Any set of consistent units is sufficient.

The initial velocities assigned to the balls, specifically (1.0 m/s, 1.0 m/s) and (-1.0 m/s, -1.0 m/s), cause them to move toward each other along the diagonal of the square. The material parameters under consideration include Young's modulus of 1,000 kPa, a Poisson's ratio of 0.3, and a density of 1.0 kg/m3. The simulation is systematically run up to a final time of t = 1.3 seconds. Figure 3.7 shows the movement of two balls in an extra illustrative scenario. Although no explicit contact law has been stated, the collision of the balls occurs in a physically realistic manner.

The mean stress distribution within the balls is rigorously tracked and observed during the collision process, as shown in Figure 3.7. Notably, no apparent stress magnitudes are recorded prior to the hit when the balls are in continual motion due to given velocities. Given the constant velocities of the material points within the balls, the absence of tension in the first phase is expected. As the collision progresses, material sites in the contact region experience increased compressive stresses, as one would expect in such a circumstance. The visual representation of stress distribution provides useful information about the dynamic behavior of elastic balls during impact.

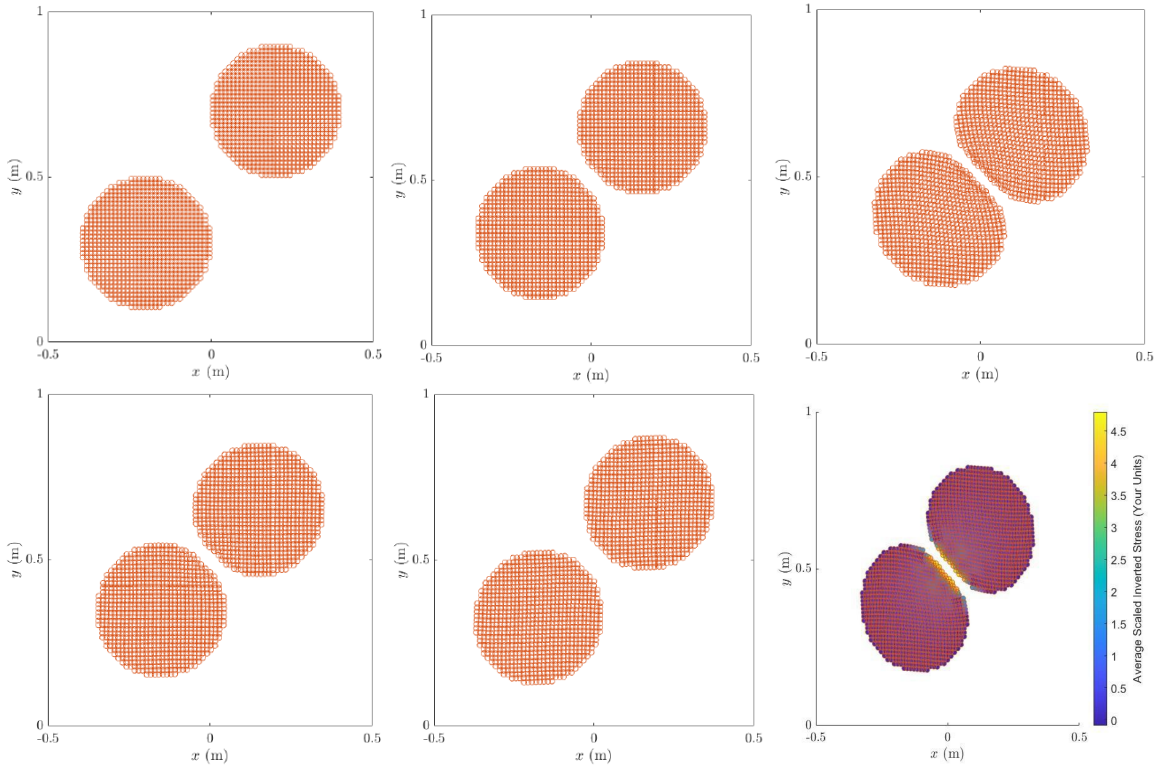

Figure 3.7 Impact of two elastic bodies: simulation snapshots. These images were created using MATLAB.

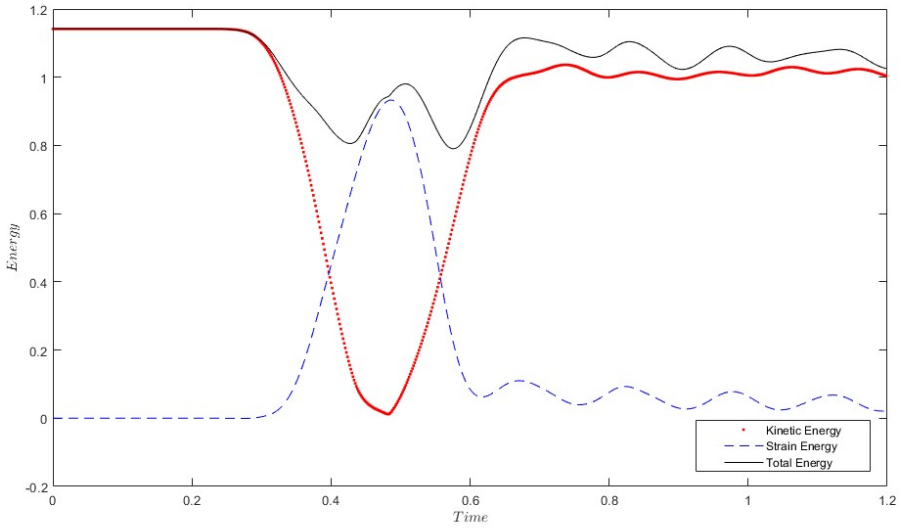

Figure 3.8 Impact of two elastic bodies: evolution of kinetic, strain, and total energies

Following the hit, Figure 3.7 shows the state of the balls post-collision. The velocities of the balls have now changed direction in comparison with their pre-collision movement. While the majority of the stress effects have subsided, tiny residual strains can still be seen on the balls. These residual stresses are due to the free vibration of the balls after the contact, emphasizing the need to include post-collision behavior in the analysis.\

Aside from measuring stress distributions, energy conservation is critical in determining the quality and dependability of simulation results. The overall energy of the system, which includes kinetic and strain energy components, is meticulously monitored. The kinetic energy (E_k) of each material point is defined by the product of its mass point (m_p) and velocity (v_p), whereas the strain energy (E_S) accounts for the strain energy stored in the material points. The energy conservation errors are studied as a function of time, specifically for a time step size of Δ_t = 0.001 seconds,

$$E_S = \sum_{p=1}^{n_p} u_p V_p$$

$$E_k = \frac{1}{2} \sum_{p=1}^{n_p} v_p \cdot v_p m_p$$

$$E_{Total} = E_S + E_k$$

where u_p denotes the strain energy density of particle p, $u_p = \frac{1}{2} \sigma_{p,ij} \epsilon_{p,ij}$

Figure 3.8 shows the evolution of kinetic, strain, and total energy during the simulation. At first, all the energy in the system is kinetic. Kinetic energy falls as the collision develops, particularly during the impact phase, and then begins to recover as the balls separate. Simultaneously, strain energy reaches its peak at the location of maximal deformation during impact and then falls to a level consistent with the ball's free vibration. These findings are consistent with earlier research, verifying the simulation methodology's application.

When the time step size is set to Δ_t = 0.001 seconds, the results demonstrate that the energy conservation errors are significant. This conclusion emphasizes the crucial importance of selecting an adequate time step size for proper collision dynamics resolution. It is especially important in the context of implicit integration methods, like the trapezoidal rule, which are known for their unconditional stability in linear analysis. However, in the current case, the need to precisely resolve the collision imposes a bound on the implicit time step size, which is referred to as the characteristic collision time.

The characteristic collision time is the time necessary for a wave to transverse one of the balls, and it depends on the wave speed and the diameter of the ball. The wave speed in this case is roughly 10.0 m/s, and the diameter of the ball is around 0.4 meters. As a result, the characteristic

collision time is projected to be 0.04 seconds, or 16 times the specified time step size. This finding highlights the difficult balance that must be struck when selecting an appropriate time step size for accurate simulation while optimizing computational performance.

Note that lowering the number of required time steps usually results in less processing time. However, because implicit and explicit integration approaches use fundamentally different solution schemes, establishing a straight one-to-one relationship between time step size and computing time reduction is difficult. Furthermore, as seen in this example, specific analysis characteristics such as wave speed and ball diameter have a considerable impact on potential reductions in the number of time steps necessary.

To summarize, the preliminary results of this study provide important insights into the dynamic analysis of collisions between elastic balls and balls utilizing the implicit dynamic approach. The element type, time step size, and contact resolution technique all play important roles in determining simulation accuracy and stability. The visual representation of stress distribution and the study of energy conservation errors provide a thorough knowledge of the simulated systems' behavior during collision. These findings pave the way for future investigation and refining of the study ideas, with a primary objective goal of improving knowledge of complicated solid mechanics problems and computational modeling methodologies.

Example: Slope Failure

Slope stability is a significant problem that geotechnical scholars have studied for many years. Analyzing slope stability is one of the many reasons to evaluate the analysis techniques that occur in the rule of mesh-based approaches that consider the effect of structure support and deformation limitations. In most cases, it is important to study the behavior of the slope beyond failure, which is unavoidable, and investigate the impact of slide masses on low-laying zones. The physical importance of slope failures can be evaluated in the form of landslides leading to a large flow of debris. Landslide-debris flow is an actual fast and massive flow-like movement of soil and fragmented rock. The impact of collapse and material mobility breakdown could cause significant damage to the residential and commercial structures that are in the flow-way. [7].

Numerous factors, including heavy rainfall, imposed loads, weathering-induced strength loss, and seismic excitation, can cause slope failures and landslides. Seismic excitation, also known as an earthquake, has been identified as the primary factor in slope failures [33]. As a result, analyzing a slope's response to a seismic event becomes more essential. To address this problem, numerous strategies have been developed. According to [31], there are three phases to evaluating a slope's performance during earthquakes: stress-deformation analysis, pseudo-static analysis, and permanent displacement analysis. When the pseudo-static analysis is used as a primary analysis method, only a limit equilibrium method representing the seismic shaking by a constant inertial force applied to a sliding mass can indicate safety against slope failure. Permanent displacement analysis is a significant improvement over pseudo-static analysis because it provides a more quantitative method for evaluating the performance of slopes during earthquakes [7].

The Newmark rigid-block analysis is a common illustration of the permanent displacement analysis [44]. In this method, the permanent displacement of a rigid block moving along an

inclined plane with a base acceleration is used to estimate the permanent slope deformation caused by earthquakes. The geometric and material models used in pseudo-static and permanent displacement analyses are extremely simplified. However, these methods cannot evaluate earthquake-induced slope deformations under complex geological conditions. For this reason, the stress-deformation investigation is utilized as it can represent complex soil behaviors (e.g., non-straight reaction to dynamic stacking, strain relaxing, and strain rate reliance on material strength) and mathematical circumstances.

It follows the approach of computing stresses in the material and its response in the form of deformations based on a defined constitutive relationship between stress and strain. A stress–deformation analysis is frequently performed using numerical methods like the FEM or finite difference method (FDM). However, the mesh-based methods (e.g., FEM) have difficulty modeling large deformations due to mesh distortion and entanglement problems. As a result, stress-deformation analysis is currently limited to estimating relatively small seismically induced slope deformations [31]. The drawback of these methods to deal with large deformations, therefore, considerably impedes their application in the analysis of earthquake-induced slope deformations.

Large deformation and failure evaluations have been a challenge for many scholars in simulating multi-phase interactions; therefore, the MPM has presented a powerful spatial assessment. In 1990, Sulsky et al. developed, presented, and applied the first MPM to model and simulate solid materials. MPM opened scholars and researchers to acknowledge the potential of the new method to be used for many different applications like silo discharge and plastic molding [56, 57]. Additionally, problems involving the effects of explosives or other large deformation [26, 29], the geotechnical quasi-static analyses of slope stability [6, 54], modeling failure, [57] anchor pull-out [13], soil column collapse [1, 36], landslides and debris flow [47], and landslide-induced interactions with structures [42] can and have been explored using MPM strategies.

The two major advantages of using MPM are the limitation of the time step and enabling improved algorithm accuracy. Addressing the time step size limitation ingrained in explicit integration schemes potentially saves major computational amounts for certain types of problems. Enabling an improved algorithm accuracy is important for various constitutive behaviors, like elastoplasticity [55].

MPM uses two discretizations. The continuum body with some of the material points carrying all the variables is the first discretization. The second, the background grid/mesh, is discretized to solve the equation of motion. To avoid the mesh deforming after the time step, the grid (a computational mesh) might be adjusted appropriately or might be maintained in its original position. This eliminates the weakness of the FEM, for which extreme grid/mesh deformation might appear due to large deformations. Like the finite element method, time integration schemes for MPM can use either explicit or implicit methodologies [55].

In the dynamic landscape of geotechnical engineering, the quest for precise simulation approaches has driven the development of the MPM. To establish a robust benchmark for the proposed MPM simulation approach, an extensive dynamic analysis of slope behavior is executed using MATLAB. The simulation unfolds over a seismic excitation period of 7.2 seconds, with the soil intricately modeled using the Mohr-Coulomb failure criterion. This section

introduces the technical intricacies and also delves into the application of MPM in the complex realm of landslide mechanics.

A critical decision surfaces regarding the choice of the domain-based TLMPM over alternatives like MUSL, justified by its superior performance in modeling torsional and stretching deformation modes. This choice is underscored by coupling TLMPM with an elastoplastic constitutive model based on non-associated Mohr-Coulomb plasticity as advocated by [65]. The study then transitions seamlessly into the analytical phase where the geometric features of the slump are meticulously analyzed. This involves a comparative study, comparing the results such as geometry and failure surface to the numerical simulation conducted by [66]. Huang et al.'s [66] approach is anchored in a Drucker–Prager model with tension cutoff (D-P), setting the stage for a nuanced evaluation.

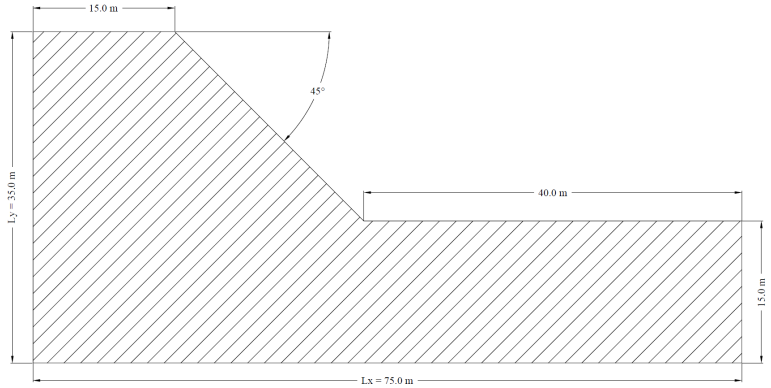

Figure 3.9 The configuration of the slump involves applying roller boundary conditions to the domain's left and right sides, with a no-slip condition enforced at the material's base.

The geometry of the problem, vividly portrayed in Figure 3.9, lays the groundwork for subsequent discussion. Here, the soil material is dissected into 75 x 35 meter elements with four material points per element, amounting to 7,031 material points. A uniform mesh spacing of 1 m is meticulously employed, with the imposition of rollers at the left and right domain limits. Simultaneously, a nonslip condition is carefully enforced at the base of the material. The procedural fidelity to [66] numerical approach, with the absence of local damping in the equation of motion and the abrupt application of gravity at the simulation's commencement, underscores the commitment to align with established methodologies.

Material properties, a cornerstone of geotechnical simulations, come to the fore with a detailed exposition. The elastoplastic cohesive material, characterized by a density $\rho = 2100$ kg/m^3, an elastic modulus $E = 70$ MPa, and a Poisson's ratio $\nu = 0.3$, encapsulates the complexity of the real-world scenario. Cohesion (c) is assigned a value of 10 Pa, and the internal friction angle (φ) stands at 20, with a conspicuous absence of dilatancy ($\delta = 0$). The total simulation time is meticulously set at 7.2 seconds, and a time step multiplier $\alpha = 0.5$ is carefully chosen.

As the narrative unfolds, the process seamlessly transitions into a critical exploration of MPM's intrinsic dissimilarity to FEM, illustrating the need for a bespoke simulation approach. Crucial revelation surfaces—prescribed velocities, a commonplace boundary condition in FEM, find no direct application in MPM simulations. This demarcation underscores the necessity for

methodological adaptations and establishes MPM as a novel paradigm in geotechnical applications, warranting a unique verification process.

The orchestration of the slope failure problem necessitates a nuanced discussion on boundary conditions, a pivotal aspect in ensuring the fidelity of the simulation. Here, the introduction of rigid particles assumes a central role in playing the part of velocity carriers. Figure 3.9 provides a visual narrative, mapping out these rigid boundaries and their nuanced interplay within the simulation. This representation extends beyond a mere technicality, underlining the essence of these rigid boundary particles as fundamental components outlining the box around the slope.

The soil's complex behavior is encapsulated in the adoption of the Mohr-Coulomb constitutive law, where the interplay of forces is meticulously modeled. A seamless transition occurs between the theoretical constructs and the practical, as the smooth contact for side boundaries emerges as a pragmatic choice. This design accommodates the free settlement of soil along the vertical direction, mirroring real-world scenarios. Simultaneously, the imposition of rough contact for the bottom in the horizontal direction introduces an additional layer of realism, bridging the theoretical and the practical with finesse.

The meticulous construction of the simulation framework, as outlined in previous sections, sets the stage for the unveiling of preliminary results. This phase ventures into the core of MPM's capabilities, illustrating its efficacy in modeling soil slopes. Mesh and particle discretizations, as visually articulated in Figure 3.10, serve as the canvas upon which the dynamics of slope behavior are painted. At t = 7.2 s, the contours of shear strain and total displacement come to life, offering a glimpse into the evolving landscape.

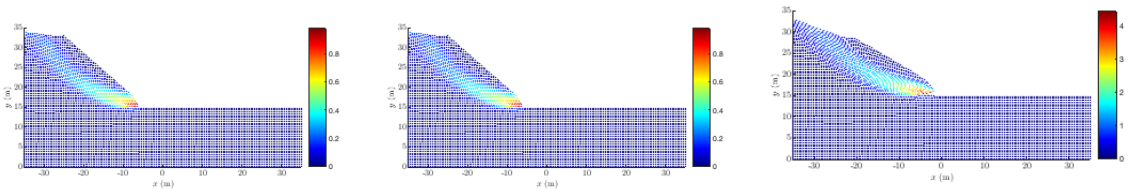

Figure 3.10 The MPM solution for the elastoplastic slump reveals the gradual development of a dynamic shear zone extending backward from the slope's toe, culminating in a circular failure mode.

Within the temporal constraints of t = 7.2 s, the deformation behavior of the slope, as predicted by MPM, aligns admirably with predictions from MATLAB and other continuum-based models. The prediction of an almost curved sliding surface resonates with the consensus within the geotechnical community. However, the imposition of a non-zero dilatancy angle of 45 degrees introduces a layer of complexity. While enhancing the prediction of the failure surface, it veers into the territory of over-predicting plastic volumetric expansion—a scenario akin to the soil undergoing heavy compaction—a contradiction to the initial state of the considered soil. This discrepancy manifests in the form of a substantial run-out distance in the numerical model.

With intellectual integrity at the forefront, the study confronts these disparities with a forward-looking lens. The acknowledgment of the inherent limitations leads to a contemplation of advanced constitutive models that intricately consider the effect of soil degradation with stress

and density evolutions. Positioned as potential refinements to the existing elastoplastic Mohr-Coulomb model, these advanced models beckon the attention of researchers and practitioners alike.

In principle, the implementation of these advanced models within the MPM framework is portrayed as a straightforward venture. However, the nuanced narrative introduces a note of caution: numerical stability problems stand as formidable challenges, and formulations are undergoing meticulous development. The saga continues with consideration of the soil's reported approximate 10% water content, introducing the proposition of amalgamating advanced constitutive models with partially saturated soil models. This hybrid approach emerges as a beacon of promise, poised to enhance the simulation of progressive failure in the experimental setting.

In Figure 3.10, the visual representation of the numerical solution to the elastoplastic problem illustrates the intricacies of slope behavior. An intense shear zone, as highlighted by the second invariant of the accumulated plastic strain, takes center stage at the toe of the slope. This zone burgeons as the material yields, propagating backward to the summit of the material, ultimately culminating in a rotational slump. The alignment of the failure surface with the [66] solution offers a semblance of validation. However, keen observations reveal disparities, notably a lower crest of the slope compared with the original work in [66].

The study navigates these distinctions with finesse, attributing the nuanced variations to the spurious material separation quandary inherent in TLMPM. The crest of the slope, subject to considerable stretching deformation modes, becomes a focal point of exploration. Despite these differences, the numerical results, resolved through vectorized and iterative solutions within approximately 7.2 seconds, resonate with the broader narrative reported by [66]. The intellectual integrity embedded in these observations opens avenues for future investigations, echoing the dynamic nature of geotechnical simulations.

This study stands as a comprehensive exploration, not merely of numerical simulations but as a journey through the intricacies of MPM in the context of geotechnical applications. Each section, meticulously woven into the fabric of the narrative, contributes to the holistic understanding of the methodology, challenges, and promises that unfold in the realm of slope dynamics.

4. SUMMARY AND CONCLUSIONS

Several material point methods have been developed and applied to problems associated with natural hazard modeling of transportation infrastructure. These include the large deformation of bridge-like structures, the impacts of particles as in rockfall or granular flows, or the gravity-driven failure of geotechnical structures. Although these problems lack comparative solutions for direct quantitative calculations, all have physically reasonable outcomes that we hope to refine and improve upon in the future.

5. REFERENCES

1. Andersen, S., & Andersen, L. (2009). "Analysis of stress updates in the material-point method." In *The Nordic Seminar on Computational Mechanics* (pp. 129–134). Department of Civil Engineering, Aalborg University.

2. Anderson Jr, C. E., & Bodner, S. R. (1988). "Ballistic impact: the status of analytical and numerical modeling." *International Journal of Impact Engineering*, *7*(1), 9–35.

3. Awal, R. (2008). "Study on landslide dam failure due to sliding and overtopping."

4. Bardenhagen, S. G., Brackbill, J. U., & Sulsky, D. (2000). "The material-point method for granular materials." *Computer Methods in Applied Mechanics and Engineering*, *187*(3–4), 529–541.

5. Benson, D. J. (1992). "Computational methods in Lagrangian and Eulerian hydrocodes." *Computer Methods in Applied Mechanics and Engineering*, *99*(2–3), 235–394.

6. Beuth, L., Więckowski, Z., & Vermeer, P. A. (2011). "Solution of quasi-static large-strain problems by the material point method." *International Journal for Numerical and Analytical Methods in Geomechanics*, *35*(13), 1451–1465.

7. Bhandari, T., Hamad, F., Moormann, C., Sharma, K. G., & Westrich, B. (2016). "Numerical modelling of seismic slope failure using MPM." *Computers and Geotechnics*, *75*, 126–134.

8. Brackbill, J. U., & Ruppel, H. M. "A Method for Adaptively Zoned, Particle-in-Cell Calculations in Two Dimensions," submitted *Journal of Computational Physics*, *1*.

9. Brackbill, J. U., Kothe, D. B., & Ruppel, H. M. (1988). "FLIP: a low-dissipation, particle-in-cell method for fluid flow." *Computer Physics Communications*, *48*(1), 25–38.

10. Camacho, G. T., & Ortiz, M. (1996). "Computational modelling of impact damage in brittle materials." *International Journal of Solids and Structures*, *33*(20–22), 2899–2938.

11. Camacho, G. T., & Ortiz, M. (1997). "Adaptive Lagrangian modelling of ballistic penetration of metallic targets." *Computer Methods in Applied Mechanics and Engineering*, *142*(3–4), 269–301.

12. Ceccato, F., Leonardi, A., Girardi, V., Simonini, P., & Pirulli, M. (2020). "Numerical and experimental investigation of saturated granular column collapse in air." *Soils and Foundations*, *60*(3), 683–696.

13. Coetzee, C. J., Vermeer, P. A., & Basson, A. H. (2005). "The modelling of anchors using the material point method." *International Journal for Numerical and Analytical Methods in Geomechanics*, *29*(9), 879–895.

14. Costa, J. E. (1991). “Documented historical landslide dams from around the world.” US. *Geological Survey Open-File Report*, *91*(239), 1–486.

15. Costa, J. E., & Schuster, R. L. (1988). “The formation and failure of natural dams.” *Geological Society of America Bulletin*, *100*(7), 1054–1068.

16. de Vaucorbeil, A., Nguyen, V. P., & Hutchinson, C. R. (2020). “A Total-Lagrangian Material Point Method for solid mechanics problems involving large deformations.” *Computer Methods in Applied Mechanics and Engineering*, *360*, 112783.

17. de Vaucorbeil, A., Nguyen, V. P., Sinaie, S., & Wu, J. Y. (2020). “Material point method after 25 years: Theory, implementation, and applications.” *Advances in Applied Mechanics*, *53*, 185–398.

18. Ermini, L., & Casagli, N. (2003). “Prediction of the behaviour of landslide dams using a geomorphological dimensionless index.” *Earth Surface Processes and Landforms: The Journal of the British Geomorphological Research Group*, *28*(1), 31–47.

19. Gingold, R. A., & Monaghan, J. J. (1977). “Smoothed particle hydrodynamics: theory and application to non-spherical stars.” *Monthly Notices of the Royal Astronomical Society*, *181*(3), 375–389.

20. Guilkey, J. E., Bardenhagen, S. G., Roessig, K. M., Brackbill, J. U., Witzel, W. M., & Foster, J. C. (2001). “Improved contact algorithm for the material point method and application to stress propagation in granular material.”

21. Guilkey, J. E., Harman, T. B., & Banerjee, B. (2007). “An Eulerian-Lagrangian approach for simulating explosions of energetic devices.” *Computers & Structures*, *85*(11–14), 660–674.

22. Guo, Y. J., & Nairn, J. A. (2006). “Three-dimensional dynamic fracture analysis using the material point method.” *Computer Modeling in Engineering and Sciences*, *16*(3), 141.

23. Han, Z. D., Liu, H. T., Rajendran, A. M., & Atluri, S. N. (2006). “The applications of meshless local Petrov-Galerkin (MLPG) approaches in high-speed impact, penetration and perforation problems.” *CMC-Tech Science Press*, *4*(2), 119.

24. Harlow, F. H. (1964). “The particle-in-cell computing method for fluid dynamics.” *Methods in Computational Physics*, *3*, 319–343.

25. Harlow, F. H. (1964). “The particle-in-cell computing method for fluid dynamics.” *Methods in Computational Physics*, *3*, 319–343.

26. Henderson, T. C., McMurtry, P. A., Smith, P. J., Voth, G. A., Wight, C. A., & Pershing, D. W. (2000). “Simulating accidental fires and explosions.” *Computing in Science & Engineering*, *2*(2), 64–76.

27. Hu, W., & Chen, Z. (2003). “A multi-mesh MPM for simulating the meshing process of spur gears.” *Computers & Structures*, *81*(20), 1991–2002.

28. Hu, W., & Chen, Z. (2006). “Model-based simulation of the synergistic effects of blast and fragmentation on a concrete wall using the MPM.” *International Journal of Impact Engineering*, *32*(12), 2066–2096.

29. Huang, P., Zhang, X., Ma, S., & Huang, X. (2011). “Contact algorithms for the material point method in impact and penetration simulation.” *International Journal for Numerical Methods in Engineering*, *85*(4), 498–517.

30. Jibson, R. W. (2011). “Methods for assessing the stability of slopes during earthquakes—A retrospective.” *Engineering Geology*, *122*(1–2), 43–50.

31. Johnson, G. R., Stryk, R. A., & Beissel, S. R. (1996). “SPH for high velocity impact computations.” *Computer Methods in Applied Mechanics and Engineering*, *139*(1–4), 347–373.

32. Keefer, D. K. (1984). “Landslides caused by earthquakes.” *Geological Society of America Bulletin*, *95*(4), 406–421.

33. Korup, O. (2004). “Geomorphometric characteristics of New Zealand landslide dams.” *Engineering Geology*, *73*(1–2), 13–35.

34. Korup, O. (2005). “Geomorphic hazard assessment of landslide dams in South Westland, New Zealand: fundamental problems and approaches.” *Geomorphology*, *66*(1–4), 167–188.

35. Kumar, K., Soga, K., & Delenne, J. Y. (2013, June). “Multi-scale modelling of granular avalanches.” In *AIP Conference Proceedings* (Vol. 1542, No. 1, pp. 1250–1253). American Institute of Physics.

36. Liszka, T., & Orkisz, J. (1980). “The finite difference method at arbitrary irregular grids and its application in applied mechanics.” *Computers & Structures*, *11*(1–2), 83–95.

37. Liu, W. K., Belytschko, T., & Chang, H. (1986). “An arbitrary Lagrangian-Eulerian finite element method for path-dependent materials.” *Computer Methods in Applied Mechanics and Engineering*, *58*(2), 227–245.

38. Lucy, L. B. (1977). “A numerical approach to the testing of the fission hypothesis.” *The Astronomical Journal*, *82*, 1013–1024.

39. Ma, S., Zhang, X., & Qiu, X. M. (2009). “Comparison study of MPM and SPH in modeling hypervelocity impact problems.” *International Journal of Impact Engineering*, *36*(2), 272–282.

40. Manville, V. (2001). *Techniques for Evaluating the Size of Potential Dam-Break Floods from Natural Dams*. Institute of Geological & Nuclear Sciences.

41. Mast, C. M. (2013). “Modeling landslide-induced flow interactions with structures using the material point method.” (Doctoral dissertation).

42. Nayroles, B., Touzot, G., & Villon, P. (1992). “Generalizing the finite element method: diffuse approximation and diffuse elements.” *Computational Mechanics*, *10*(5), 307–318.

43. Newmark, N. M. (1965). “Effects of earthquakes on dams and embankments.” *Geotechnique*, *15*(2), 139–160.

44. Scheffler, D. R. (2005). “Modeling non-eroding perforation of an oblique aluminum target using the Eulerian CTH hydrocode.” *International Journal of Impact Engineering*, *32*(1-4), 461–472.

45. Schuster, R. L. (2000). “Outburst debris-flows from failure of natural dams.” In *Debris flow hazards mitigation—Mechanics, prediction, and assessment* (pp. 29–42).

46. Shin, W. K. (2009). *Numerical simulation of landslides and debris flows using an enhanced material point method*. University of Washington.

47. Silling, S. A. (1992). “Eulerian Simulation of the Perforation of Aluminum Plates by Nondeforming Projectiles” (No. SAND-92-0493). Sandia National Labs., Albuquerque, NM (United States).

48. Sulsky, D., & Kaul, A. (2004). “Implicit dynamics in the material-point method.” *Computer Methods in Applied Mechanics and Engineering*, *193*(12–14), 1137–1170.

49. Sulsky, D., & Schreyer, H. L. (1996). “Axisymmetric form of the material point method with applications to upsetting and Taylor impact problems.” *Computer Methods in Applied Mechanics and Engineering*, *139*(1–4), 409–429.

50. Sulsky, D., Chen, Z., & Schreyer, H. L. (1994). “A particle method for history-dependent materials.” *Computer Methods in Applied Mechanics and Engineering*, *118*(1–2), 179–196.

51. Sulsky, D., Zhou, S. J., & Schreyer, H. L. (1995). “Application of a particle-in-cell method to solid mechanics.” *Computer Physics Communications*, *87*(1-2), 236–252.

52. Tan, H., & Nairn, J. A. (2002). “Hierarchical, adaptive, material point method for dynamic energy release rate calculations.” *Computer Methods in Applied Mechanics and Engineering*, *191*(19-20), 2123–2137.

53. Wang, B., Vardon, P. J., & Hicks, M. A. (2013). “Implementation of a quasi-static material point method for geotechnical applications.” In *Computational Geomechanics, COMGEO III,* Krakow, Poland (pp. 305–313). IC2E-International Centre for Computational Engineering.

54. Wang, B., Vardon, P. J., Hicks, M. A., & Chen, Z. (2016). “Development of an implicit material point method for geotechnical applications.: *Computers and Geotechnics*, *71*, 159–167.

55. Więckowski, Z. (2004). “The material point method in large strain engineering problems.” *Computer Methods in Applied Mechanics and Engineering*, *193*(39–41), 4417–4438.

56. Więckowski, Z., Youn, S. K., & Yeon, J. H. (1999). “A particle-in-cell solution to the silo discharging problem.” *International Journal for Numerical Methods in Engineering*, *45*(9), 1203–1225.

57. Xiao-Fei, P., Ai-Guo, X., Guang-Cai, Z., Ping, Z., Jian-Shi, Z., Shang, M., & Xiong, Z. (2008). “Three-dimensional multi-mesh material point method for solving collision problems.” *Communications in Theoretical Physics*, *49*(5), 1129.

58. York, A. R., Sulsky, D., & Schreyer, H. L. (1999). “The material point method for simulation of thin membranes.” *International Journal for Numerical Methods in Engineering*, *44*(10), 1429–1456.

59. Zhang, H. W., Wang, K. P., & Chen, Z. (2009). “Material point method for dynamic analysis of saturated porous media under external contact/impact of solid bodies.” *Computer Methods in Applied Mechanics and Engineering*, *198*(17–20), 1456–1472.

60. Zhang, X., Sze, K. Y., & Ma, S. (2006). “An explicit material point finite element method for hyper-velocity impact.” *International Journal for Numerical Methods in Engineering*, *66*(4), 689–706.

61. Randles, P. W., & Libersky, L. D. (1996). “Smoothed particle hydrodynamics: Some recent improvements and applications.” *Computer Methods in Applied Mechanics and Engineering*, 139(1–4), 375–408.

62. Sulsky, D., & Brackbill, J. U. (1991). “A numerical method for suspension flow.” *Journal of Computational Physics*, 96(2), 339–368.

63. York, A. R. (1997). “Development of modifications to the material point method for the simulation of thin membranes, compressible fluids, and their interactions” (Unpublished doctoral dissertation). The University of New Mexico, Albuquerque.

64. Simpson, G. *Practical Finite Element Modeling in Earth Science Using Matlab*. Wiley Online Library, 2017.

65. Huang, P., Li, S.-l., Guo, H., & Hao, Z.-m. “Large deformation failure analysis of the soil slope based on the material point method.” *Computers & Geosciences*, 19, 951–963, 2015.

66. Timoshenko, S., & Goodier, J. N. *Theory of Elasticity*. McGraw-Hill Book Company. Inc., New York, 1951.

67. S. Chucheepsakul, Suraphan Buncharoen, & T. Huang. "Elastica of Simple Variable-Arc-Length Beam Subjected to End Moment." *Journal of Engineering Mechanics* 121 (July) 767–772, 1995.

68. Ma, H. M., X. L. Gao, & J. N. Reddy. "A microstructure-dependent Timoshenko beam model based on a modified couple stress theory." *Journal of the Mechanics and Physics of Solids*, 56(12) 3379–3391, 2008.

69. Andersen, S., & L. Andersen. "Material-point method analysis of bending in elastic beams." *Proceedings of the 11th International Conference on Civil, Structural and Environmental Engineering Computing*, Civil-Comp 2007, (7), 2007.